energies

MDPI

Article

Experimental and Modelling Study on the Performance of an SI Methanol Marine Engine Under Lean Conditions

Shishuo Gong [1], Weijie Liu [1,2,3,*], Junbo Luo [1], Zhou Fang [1] and Xiang Gao [1,2,3]

[1] State Key Lab of Clean Energy Utilization, State Environmental Protection Engineering Center for Coal-Fired Air Pollution Control, Zhejiang University, Hangzhou 310027, China; xgao1@zju.edu.cn (X.G.)
[2] Zhejiang Baima Lake Laboratory, Hangzhou 310051, China
[3] Jiaxing Research Institute, Zhejiang University, Jiaxing 314000, China
* Correspondence: liuwj2023@zju.edu.cn

Abstract

This study presents the experimental and modelling investigation of the performance of an SI methanol marine engine operating under lean conditions. The effects of spark timing and excess air ratio on combustion characteristics, engine performance, and emissions are explored. Multiple machine learning models, including Support Vector Machines (SVM), Artificial Neural Network (ANN), LightGBM, and Random Forest (RF), are employed to predict the engine performance and emission characteristics. Experimental results show that as spark timing advances, the combustion phase advances, with the burn duration being extended. When the excess air ratio is less than 1.35, there exists an optimal spark timing, corresponding to a maximum brake thermal efficiency. The optimal spark timing exhibits an advancing tendency along with increasing excess air ratio. HC emission is primarily determined by the excess air ratio and shows no significant variation under the different spark timings. NO_x emission is initially increased and then decreased with advancing spark timing. Compared with ANN, LightGBM, and RF, SVM demonstrates a superior predictive accuracy, with R^2 values for engine performance exceeding 0.98 and R^2 values for emissions above 0.92.

Keywords: SI methanol marine engine; lean combustion; spark timing; excess air ratio

check for updates

Academic Editor: Roberto Finesso

Received: 13 October 2025
Revised: 6 November 2025
Accepted: 13 November 2025
Published: 18 December 2025

Citation: Gong, S.; Liu, W.; Luo, J.; Fang, Z.; Gao, X. Experimental and Modelling Study on the Performance of an SI Methanol Marine Engine Under Lean Conditions. *Energies* **2025**, *18*, 6607. https://doi.org/10.3390/en18246607

Copyright: © 2025 by the authors. Licensee MDPI, Basel, Switzerland. This article is an open access article distributed under the terms and conditions of the Creative Commons Attribution (CC BY) license (https://creativecommons.org/licenses/by/4.0/).

1. Introduction

Maritime shipping accounts for more than 80% of global international freight traffic, making it a major contributor to global greenhouse gas (GHG) emissions [1]. To address GHG emissions from maritime shipping, the International Maritime Organization aims to achieve net-zero GHG emissions from the global shipping industry by around 2050. The EU's Fit for 55 proposes a reduction of at least 55% in GHG emissions by 2030 [2]. As regulations are increasingly stringent, developing alternative fuels has become an effective way to achieve GHG reductions [3,4].

Methanol has emerged as a promising alternative fuel [5]. The low heating value of methanol is 20.06 MJ/kg, while the octane number is 109. The characteristics of methanol, including high octane number, high laminar flame speed, and large latent heat of vaporization [6–8], provide the engine with high anti-knock capability, enhanced efficiency, and low emissions. Zhu et al. [9] found that the brake thermal efficiency (BTE) increased by 3% and COV_{IMEP} was kept below 2% when methanol was applied to an SI natural gas engine. Chen et al. [10] revealed that the peaks of in-cylinder pressure and heat release rate were highest

when fueled with methanol, as compared to ethanol and n-butanol. In recent years, lean combustion has served as an effective strategy to further enhance the thermal efficiency and the emission characteristics in methanol-fueled engines [11,12]. Zhao et al. [13] reported that the indicated thermal efficiency (ITE) of the engine fueled by methanol increased by 2.39% and NOx emission decreased by 72.17% under an optimal excess air ratio. Kim et al. [14] determined that lean burning could reduce specific fuel consumption by up to 27.5% and NOx emissions by up to 83.4% in a direct injection engine. With the ability to enhance efficiency and reduce emissions, methanol also exhibits considerable potential as a clean and efficient fuel for marine engines.

Methanol is predominantly utilized in a dual-fuel mode for marine engines. Engine control parameters, including spark timing, injection timing, and excess air ratio, significantly influence the combustion characteristics, engine performance, and emissions of the methanol engine. Gong et al. [15] numerically found that delaying spark timing could reduce NO emissions, but CO, methanol, and formaldehyde emissions increased. Duan et al. [16] proved that delaying injection timing could reduce NO emissions but increase CO, methanol, and formaldehyde emissions. They also concluded that delaying spark timing could reduce CO and NO emissions but lead to a reduction in BTE. Ning et al. [17] reported that increasing the methanol substitution rate and delaying the methanol injection timing could improve engine BTE, while reducing THC and CO emissions. Yin et al. [18] investigated the engine operating range and performance under different methanol energy substitution ratio (ESR) conditions. The results indicated that the maximum ESR can reach 65.1% at full engine load, and the maximum ESR under 79.5% load condition could reach 52.4%. Current research on methanol marine engines mainly focuses on dual-fuel combustion, while studies on pure methanol operation remain limited. Further research is required to investigate the impact of key parameters on the performance of pure methanol marine engines.

The large number of key parameters leads to prolonged experimental cycles and increased procedural complexity in investigating their impact on engine performance. Consequently, the application of machine learning to enable rapid and accurate prediction of the effects on engine performance has become a hot topic of research. Amin et al. [19] employed an ANN to predict the impact of fuel composition on engine performance, achieving high accuracy with close agreement between the predicted and experimental data. Wang et al. [20] constructed the SVM-based model to predict engine cycle variations. Using a genetic algorithm, the model achieved high predictive accuracy, attaining an R^2 value of 0.9972 and a mean squared error of 0.0197 for $CoV_{CA10\text{-}90}$. Rahimi et al. [21] developed a wavelet neural network (WNN) coupled with a stochastic gradient algorithm (SGA) to predict performance and exhaust emissions, obtaining satisfactory results. However, different machine learning models exhibit varying applicability. It is necessary to develop machine learning models according to operating conditions for improving both predictive accuracy and efficiency.

This study presents an experimental and modelling study on the performance of an SI methanol marine engine under lean conditions. Experiments were conducted on a methanol marine engine to investigate the effects of spark timing and excess air ratio on combustion characteristics, engine performance, and emissions. Machine learning was employed to construct predictive models of engine performance based on experimental measurements. A comparative analysis was conducted to evaluate the predictive accuracy of four machine learning models. In this paper, the experimental setup, test procedure, and predictive models are presented in Section 2. Section 3 outlines the effects of key parameters on the combustion characteristics, engine performance, and emissions. Additionally, the predictive accuracy of different models is compared. The results are expected to optimize

the BTE and emission characteristics of methanol marine engines, while providing an accurate predictive model to shorten experimental cycles.

2. Methodology

2.1. Experimental Setup

A schematic diagram of the experimental setup is shown in Figure 1. The experimental setup includes a modified engine, fuel supply system, control system, and measurement system. The experiments were conducted on a four-cylinder, four-stroke, naturally aspirated SI engine modified from a marine diesel engine. The major modifications included adjusting the compression ratio from 17:1 to 12.5:1 to avoid knocking in the methanol engine, mounting spark plugs at diesel injector holes, installing methanol injectors on the intake manifold, and installing an oxygen sensor on the exhaust manifold. The detailed engine parameters are shown in Table 1. Methanol was delivered to the port injection rail and injectors via N_2 pressurization. The spark timing (ST), injection parameters, and excess air ratio (λ) were controlled by an electronic control unit (ECU).

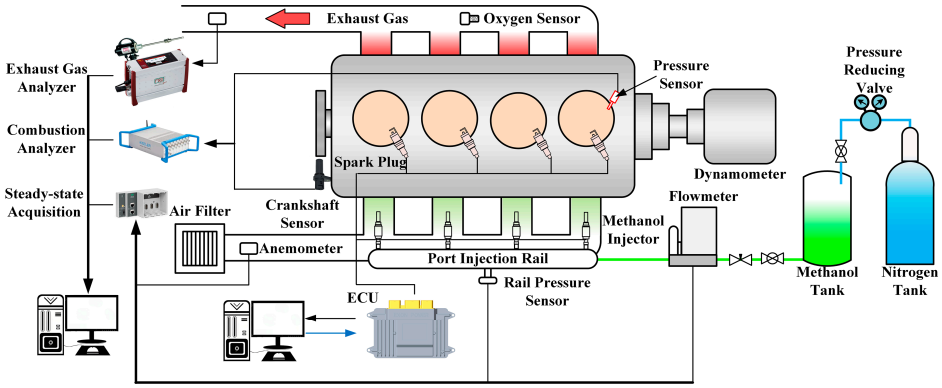


Figure 1. Schematic diagram of the experimental setup.

Table 1. Engine specifications.

Parameters	Specification
Number of cylinders	Inline 4-cylinder
Displacement (L)	4.214
Bore (mm)	108
Stroke (mm)	115
Compression ratio	12.5:1
Number of valves	2
IVO/IVC (°CA aTDC)	327/606
EVO/EVC (°CA aTDC)	114/378

The dynamometer was directly coupled with the test engine to load and measure the engine torque and speed. A flowmeter (CODA KC Series, Alicat from Shanghai, China) was utilized to measure the consumption of methanol. The in-cylinder pressure data was captured by a pressure sensor (6054BR, Kistler from Shanghai, China) with a resolution of 0.1 °CA. Subsequently, the data with 200 cycles was processed in a combustion analyzer (Kibox2, Kistler from Shanghai, China). The emissions data was sampled by an exhaust gas analyzer (MGA6, MRU from Beijing, China).

In this article, the engine speed was maintained at 1400 rpm, and the coolant temperature was maintained at 348 ± 5 K. The experiment was conducted at room temperature and atmospheric pressure. The methanol injection pressure was set to 0.9 MPa. The methanol injection pulse width was kept at 9 ms with a single injection per cycle. Various experiments

were conducted under excess air ratios ranging from 1.0 to 1.4. Meanwhile, spark timing was swept from −21 °CA aTDC to −45 °CA aTDC with an increment of 3 °CA aTDC. The operation conditions are summarized in Table 2.

Table 2. Operating conditions.

Parameters	Value
Engine speed (rpm)	1400
Excess air ratio	1.0~1.4
Spark timing (°CA aTDC)	−21~−45
Coolant temperature (K)	348 ± 5
End of injection (°CA aTDC)	−240
Intake pressure (bar)	1.0
Injection pressure (MPa)	0.9
Injection pulse width (ms)	1400

2.2. Data Processing

Heat release rate (*HRR*) is calculated using cylinder pressure and cylinder volume according to [22]

$$HRR = \frac{k}{k-1} p \frac{dV}{d\theta} + \frac{1}{k-1} V \frac{dp}{d\theta} \quad (1)$$

where k is the specific heat ratio, V is the cylinder volume, θ is the crankshaft angle, and p is the in-cylinder pressure.

Brake thermal efficiency (*BTE*) is defined as the ratio of effective work to total fuel heat value. *BTE* can be calculated by following [23]:

$$BTE = \frac{W}{m_{methanol} \times LHV_{methanol}} \quad (2)$$

where W is the brake work, $m_{methanol}$ is the mass of methanol injection per second, and $LHV_{methanol}$ is the low heat value of methanol.

The indicated mean effective pressure (*IMEP*), defined as the indicated work per unit volume per cycle, is used to evaluate the utilization of the cylinder working volume and can be calculated by following [24]:

$$IMEP = W_i / V_d \quad (3)$$

$$W_i = \int pdV \quad (4)$$

where V_d is the cylinder displacement, W_i is the indicated work per cycle.

The coefficient of variation in *IMEP* (COV_{IMEP}) is used to evaluate the combustion stability and can be calculated by following [25]:

$$COV_{IMEP} = \frac{\sigma_{IMEP}}{M_{IMEP}} \times 100\% \quad (5)$$

$$\sigma_{IMEP} = \sqrt{\frac{\sum_{i=1}^{n} (IMEP_i - M_{IMEP})^2}{n-1}} \quad (6)$$

$$M_{IMEP} = \frac{\sum_{i=1}^{n} IMEP_i}{n} \quad (7)$$

where σ_{IMEP} is the standard deviation of IMEP, M_{IMEP} is the mean of IMEP, $IMEP_i$ is the IMEP value for a particular cycle, and n represents the number of cylinder pressure data points collected for each operating condition, which is 200 in this study.

2.3. Machine Learning Models of the Methanol Engine

Machine learning methods were applied to predict the performance of the engine. In this study, Support Vector Machines (SVM), Artificial Neural Network (ANN), and LightGBM were employed to predict the engine performance and emission characteristics based on experimental data. Five controllable parameters: the engine speed, spark timing, air flow rate, methanol heat release rate (per second), and calorific value of methanol were employed as inputs. The outputs of the model include engine performance (brake torque, brake power, BTE, BSFC), and emissions (HC, NOx).

SVM is a supervised learning algorithm commonly employed for both classification and regression tasks. By introducing kernel functions, SVM can be used for high-dimensional linear problems [26]. Based on the Karush–Kuhn–Tucker condition and kernel tricks, the original linear regression function can be converted into a nonlinear function. In this study, the radial basis function is employed as a kernel function. Both the regularization parameter C and kernel coefficient γ are sampled from a log-uniform distribution. C is within the range of 1 and 1000 while γ is within the range of 0.0001 and 0.1. The solution function for nonlinear regression problems can be expressed as

$$f(x) = \sum_{i=1}^{N} (\alpha_i - \alpha_i^*) K(x_i \cdot x_i^*) + b \tag{8}$$

where x_i is the support vector, N is the number of support vectors, and $K(x_i \cdot x_i^*)$ is the kernel function.

The Gaussian kernel function is used:

$$K(x_i, x_j) = exp(-x_i - x_j^2) \tag{9}$$

where x_i and x_j represent feature vectors.

ANN is a machine learning model inspired by the structure of biological neurons. It is widely used in tasks such as classification, regression, and pattern recognition. In this paper, ANN consisted of an input layer, two hidden layers, and an output layer. Each hidden layer comprised 32 neurons. The mathematical formula for the ANN can be expressed as [27]

$$y = f(\sum_{i=1}^{N} w_i x_i - \theta) \tag{10}$$

where w_i is the input node, x_i is the weight, θ is the threshold, f is the activation function, and y represents the output.

The Sigmoid function is used as the activation function to introduce a nonlinear relationship:

$$f(x) = \frac{1}{1 + e^{-x}} \tag{11}$$

LightGBM is a machine learning algorithm based on the gradient boosting decision tree (GBDT) framework [28]. It integrates multiple weak decision trees to gradually fit residuals and improve the predictive performance of the model. In this study, LightGBM model was developed based on Gradient Boosting Decision Trees, with a learning rate of 0.05, a maximum of 15 leaf nodes, and a maximum tree depth of 4. This configuration

effectively mitigated overfitting while maintaining the model's learning capability. The prediction results can be expressed as

$$f(x) = \sum_{i=1}^{N} w(x) \tag{12}$$

where $f(x)$ is the sum of the output values $w(x)$ of all decision trees.

RF is an ensemble learning algorithm proposed by Breiman. It constructs multiple decision trees and averages their results [29]. In this study, the random forest model consisted of 100 decision trees without constraints on maximum tree depth. The final prediction result can be expressed as

$$h(x) = \frac{1}{N}\sum_{i}^{N} h(x, \theta_i) \tag{13}$$

where $h(x)$ is the model prediction result, N is the number of decision trees, x is the input feature vector of the model, θ_i is the randomly distributed feature vector, and $h(x, \theta_i)$ is the prediction result based on x and θ_i.

A total of 612 experimental datasets were employed to train and validate the machine learning models. To optimize data utilization and improve prediction accuracy, experimental data with CO levels exceeding 6000 ppm were identified as outliers and removed from the dataset during preprocessing. The inputs and outputs were standardized to zero mean and unit variance based on their respective characteristics. The experimental data were randomly divided into a training set (80%) and a test set (20%) to ensure a reliable evaluation of the model's performance on unseen data. Considering the limited size of the experimental dataset, 3-fold cross-validation was employed to evaluate the model's generalization capability.

The coefficient of determination (R^2) and root mean square error (*RMSE*) were selected as evaluation indicators for the model in this study. R^2 was used to measure the model's ability to explain fluctuations in the output variable, with a value range of [0, 1]. The closer the value is to 1, the better the model fits. *RMSE* represents the average error between the predicted value and the actual value. Smaller values indicate higher model prediction accuracy. The formulas for R^2 and *RMSE* are shown below:

$$R^2 = \frac{\sum_{i=1}^{N} (\hat{y}_i - \overline{y})^2}{\sum_{i=1}^{N} (y_i - \overline{y})^2} \tag{14}$$

$$RMSE = \sqrt{\frac{1}{N}\sum_{i=1}^{N} (y_i - \overline{y})^2} \tag{15}$$

where $\hat{y}_i$ is the predicted value, y_i is the actual value, and $\overline{y}$ is the average of actual values.

3. Results and Discussion

3.1. Combustion Characteristics

Figure 2 shows the curves of in-cylinder pressure and heat release rate at different spark timings and excess air ratios. Figure 2a plots the variation in in-cylinder pressure and HRR under different spark timings when the excess air ratio is 1.2. It is observed that the peak of in-cylinder pressure increases while the peak of HRR decreases gradually with the advance in spark timing. The combustion phase moves toward top dead centre (TDC) as

spark timing advances, resulting in a more isochoric combustion and an increasing peak of in-cylinder pressure [30]. The in-cylinder pressure and HRR traces shift to TDC, while the shape of the cylinder pressure and HRR traces undergo insignificant changes with spark timing advancing. An exception is observed at ST = −21 °CA aTDC, where the initiation of combustion is shifted into the decline phase of in-cylinder pressure, leading to a bimodal in-cylinder pressure trace.

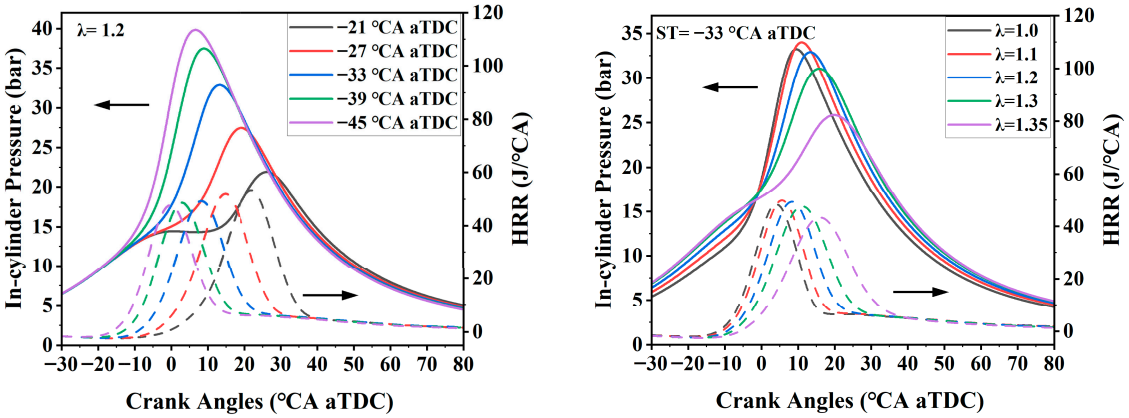


Figure 2. In-cylinder pressure and heat release rate at different (**a**) spark timings and (**b**) excess air ratios.

The in-cylinder pressure and HRR curves at different excess air ratios under the spark timing of −33 °CA aTDC are presented in Figure 2b. The peaks of in-cylinder pressure and HRR are observed to increase with excess air ratio ranging from 1.0 to 1.1. However, a gradual decline is observed as the excess air ratio increases from 1.1 to 1.35. Lean combustion reduces flame propagation velocity with increasing excess air ratio, resulting in broadened traces of in-cylinder pressure and HRR with delayed peaks [31].

Figure 3 demonstrates the effect of spark timing and excess air ratio on the maximums of in-cylinder pressure (P_{max}) and HRR (HRR_{max}) with corresponding crank angles. As shown in Figure 3a, P_{max} monotonically increases with spark timing advancing under all excess air ratio conditions. As the excess air ratio increases from 1.0 to 1.35, P_{max} initially increases and then decreases. Specifically, P_{max} reaches the maximum at λ = 1.1 for ST = −21 °CA aTDC to −36 °CA aTDC and at λ = 1.2 for ST = −39 °CA aTDC to −45 °CA aTDC. However, excessive intake leads to an over-lean mixture, resulting in a reduction of P_{max}. P_{max} crank angle advances with advancing spark timing, while it delays as the excess air ratio increases. Severe combustion instability is observed at a spark timing of −21 °CA aTDC and the excess air ratio of 1.35. Correspondingly, P_{max} occurring near TDC is generated by the piston compression rather than by combustion.

It can be determined from Figure 3b that HRR_{max} gradually decreases with advancing spark timing for the excess air ratio ranging from 1.0 to 1.3. This is due to the fact that burn duration increases with advancing spark timing, resulting in a reduction in the HRR_{max}. An exception is observed at the excess air ratio of 1.35. The volumetric fuel concentration increases with the spark timing advancing, resulting in a gradual rise of HRR_{max}. As the excess air ratio increases from 1.0 to 1.35, HRR_{max} initially increases and then decreases. HRR_{max} crank angle advances with advancing spark timing, while it is delayed as the excess air ratio increases. HRR_{max} is observed to be much lower when spark timing is −21 °CA aTDC, and the excess air ratio is 1.35 due to combustion instability.

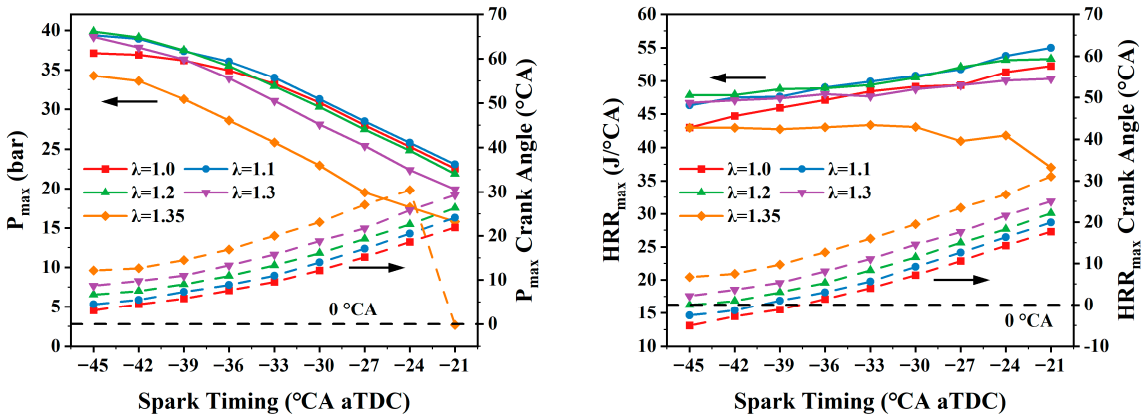


Figure 3. Effect of (**a**) spark timing and (**b**) excess air ratio on P_{max} and HRR_{max} with corresponding crank angles.

The start and end points of combustion are defined as 5% (CA05) and 90% (CA90) of the cumulative heat release, respectively. Figure 4 presents the combustion phases under different spark timings and excess air ratios. The effect of spark timing on the entire combustion process under the excess air ratio of 1.2 is illustrated in Figure 4a. The entire combustion process is extended by 33% as spark timing advances from −21 °CA aTDC to −45 °CA aTDC. CA05 advances from after to before TDC with advanced spark timing, while the crank angle of CA90 exhibits no significant variation. During the entire combustion process, the proportion of ignition delay decreases from 49.8% to 41.9%, the proportion of CA05-CA50 drops from 15.8% to 11.7%, while the proportion of CA50-CA90 increases from 34.4% to 46.4%.

As shown in Figure 4b, ignition delay shows no significant variation when spark timing advances from −21 °CA aTDC to −33 °CA aTDC, while it gradually increases with further advanced spark timing. As spark timing advances, the in-cylinder temperature and pressure have not reached the optimal levels when the spark discharge occurs, which slows the formation of a fireball and consequently prolongs ignition delay [32]. Ignition delay is prolonged as the excess air ratio increases from 1.0 to 1.35. The increase in excess air ratio reduces the concentration of methanol and decreases flame propagation velocity, resulting in an increase in ignition delay.

The variations in CA05-CA50 and CA50-CA90 under different spark timings and excess air ratios are presented in Figure 4c. CA05-CA50 is not significantly affected by spark timing when the excess air ratio ranges from 1.0 to 1.2. When the access air ratio is 1.3 and 1.35, the earlier initiation of combustion leads to elevated in-cylinder temperature and pressure during the compression stroke, which accelerates the combustion rate and shortens the duration of CA05-CA50. As the excess air ratio increases, the reduced flame propagation velocity prolongs CA05-CA50 with increasing excess air ratio. CA50-CA90 is observed to increase with advancing spark timing under all excess air ratio conditions. The advancing spark timing shifts CA05-CA50 closer to TDC, which reduces combustion intensity during the power stroke. Consequently, the in-cylinder pressure declines more rapidly during the power stroke, extending the duration of CA50-CA90. CA50-CA90 decreases as the excess air ratio increases from 1.0 to 1.35. The oxygen concentration promotes the oxidation of methanol combustion intermediates and shortens the CA50-CA90. Compared with CA05-CA50, CA50-CA90 exhibits high sensitivity to both spark timing and excess air ratio, resulting in an extension of burn duration with advancing spark timing and a reduction with increasing excess air ratio, as shown in Figure 4d.

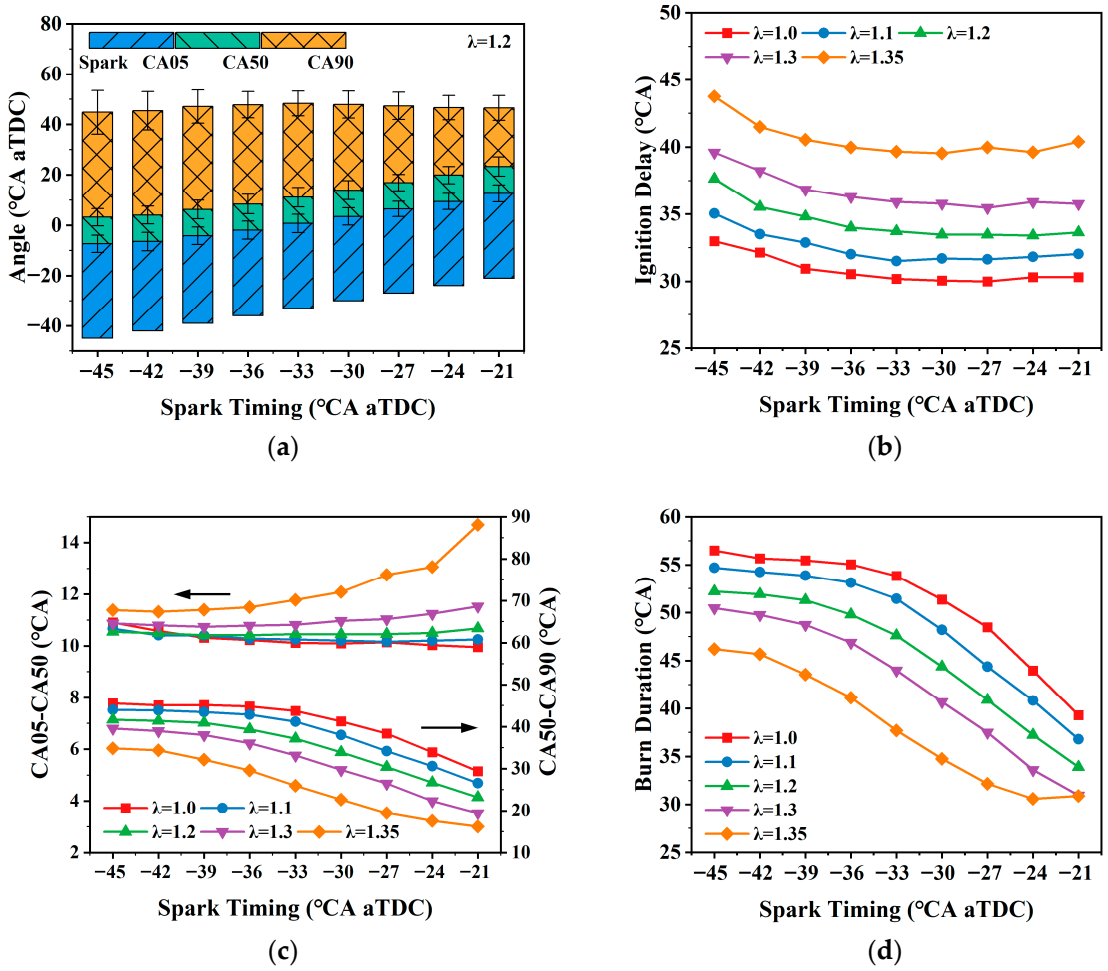


Figure 4. Effect of spark timing and excess air ratio on (**a**) the entire combustion process, (**b**) ignition delay, (**c**) CA05-CA50 and CA50-CA90, and (**d**) burn duration.

Figure 5 shows the effect of spark timing and excess air ratio on IMEP and COV_{IMEP}. In this study, COV_{IMEP} = 5% is defined as the threshold for stable combustion in the cylinder [33]. Within the excess air ratio ranging from 1.0 to 1.3, an optimal spark timing maximizing IMEP is observed at −33, −33, −36, and −39 °CA aTDC under the corresponding excess air ratios. Meanwhile, a consistent increase in IMEP is obtained with rising excess air ratio. Advancing spark timing beyond the optimum point generates excessively high in-cylinder pressure during the compression stroke, which increases negative work and consequently reduces IMEP [34]. At an excess air ratio of 1.35, negative work is reduced by the lean mixture, allowing IMEP to monotonically increase with advancing spark timing. Within the excess air ratio range of 1.0 to 1.3, COV_{IMEP} is initially decreased and then slightly increased with spark timing delay. However, at the excess air ratio of 1.35 and spark timing of −21 °CA aTDC, unstable combustion is induced by the lean mixture combined with delayed ignition, resulting in a significant increase in COV_{IMEP}.

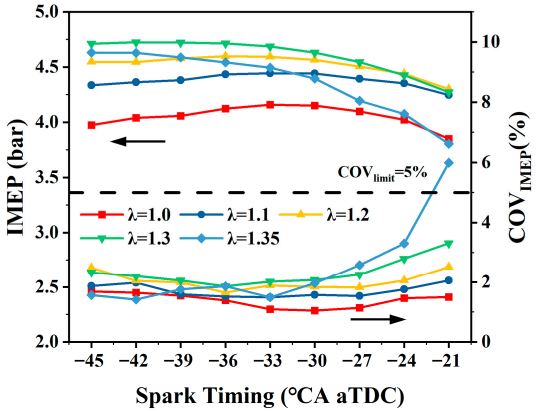


Figure 5. Effects of spark timing and excess air ratio on IMEP and COV_{IMEP}.

3.2. Engine Performance and Emission Characteristics

The contour plot illustrating engine BTE under different spark timings and excess air ratios is presented in Figure 6. It can be seen that the engine BTE generally increases with advancing spark timing and increasing excess air ratio. Under the excess air ratio of 1.4 and the spark timing of −45 °CA aTDC, the methanol engine exhibits the maximum BTE. BTE initially increases and then decreases with spark timing advancing when the excess air ratio is less than 1.35. Earlier spark timing results in higher pressure in the compression stroke, while later spark timing leads to increased exhaust loss, both reducing the BTE [35]. As the excess air ratio advances within this range, an optimum spark timing that maximizes BTE (BTE_{max}) is observed for each condition. When the excess air ratio exceeds 1.35, the piston's negative work is reduced by the lean mixture, resulting in a monotonic increase in BTE. As the excess air ratio increases, BTE_{max} exhibits an increasing trend due to the increased mass of air in the cylinder and the enhanced combustion [36], with the corresponding optimum spark timing showing an advance tendency. As the excess air ratio increases from 1.0 to 1.4, BTE_{max} is observed to increase by 5.9%, with the corresponding optimum spark timing advancing from −33 °CA aTDC to −45 °CA aTDC.

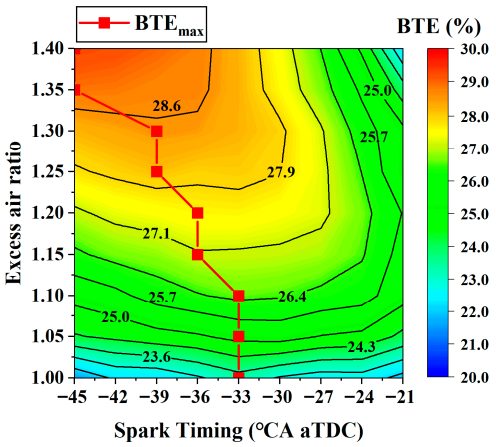


Figure 6. Variation in BTE under different spark timings and excess air ratios.

The energy distribution is analyzed to further investigate the trend of engine thermal efficiency. The total calorific value of methanol is partitioned into five parts: incomplete combustion loss, heat transfer loss, pumping, friction, and BTE. Figure 7 shows the effect of spark timing and excess air ratio on the engine energy balance. As shown in Figure 7a, the incomplete combustion loss generally increases as spark timing advances at the excess air ratio of 1.2. In this study, the incomplete combustion loss primarily included unburned

methanol, methanol escape, and the wet-wall phenomenon. The high incomplete combustion loss is primarily attributed to the occurrence of the wet-wall phenomenon. The heat transfer loss includes exhaust heat loss and coolant heat loss. As spark timing advances from −21 °CA aTDC to −45 °CA aTDC, the heat transfer loss is decreased by 5.4%. Pumping and friction exhibit negligible variation with spark timing advancing. This indicates that the initial increase in BTE with advancing spark timing is primarily driven by the reduction in heat transfer loss. And the subsequent decrease is predominantly attributed to the rise in incomplete combustion loss.

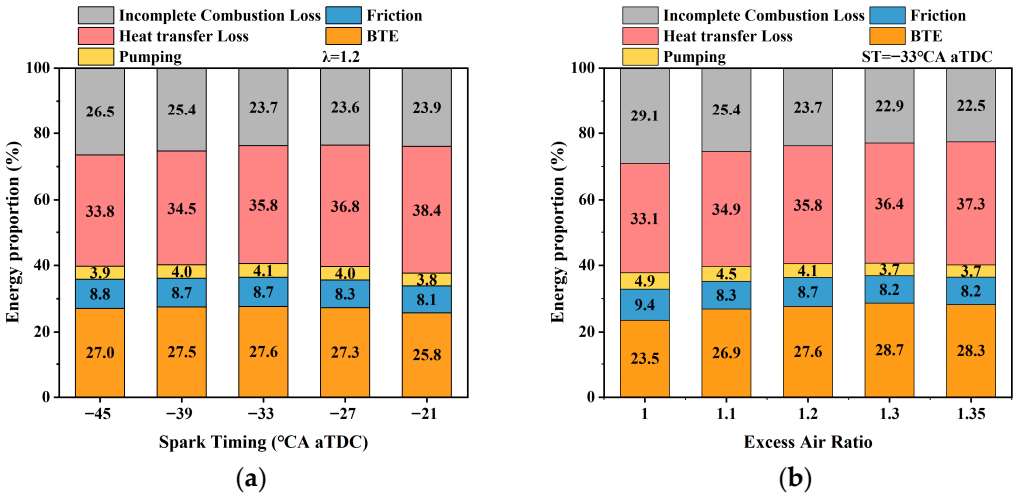


Figure 7. Energy balance at different (**a**) spark timing and (**b**) excess air ratio.

As shown in Figure 7b, at the spark timing of −33 °CA aTDC, increasing the excess air ratio from 1.0 to 1.35 provides sufficient oxygen, promoting fuel combustion and reducing incomplete combustion loss by 6.6%. Meanwhile, the heat transfer loss increased by 4.2%. Raising the throttle opening increases the intake air resistance and reduces pumping. Under lean conditions, the in-cylinder pressure during the compression stroke is reduced, decreasing piston load and friction. These observations indicate that the improvement of BTE under lean conditions is primarily attributed to reductions in incomplete combustion loss, pumping, and friction. BTE is observed slightly lower at the excess air ratio of 1.35, owing to increased heat transfer loss.

Figure 8 illustrates the impact of spark timing and excess air ratio on HC and NOx emissions. As shown in Figure 8a, the effect of spark timing on HC emission varies under different excess air ratios. When the excess air ratio ranges from 1.0 to 1.1, the in-cylinder fuel concentration is relatively high, and HC emission is reduced with spark timing advancing. At the excess air ratio of 1.2, advancing spark timing under lean conditions lowers exhaust gas temperature, which hinders HC oxidation [16], resulting in increased HC emission. When the excess air ratio ranges from 1.3 to 1.35, a non-significant variation in HC emission is observed with advancing spark timing. Compared with spark timing, HC emission is primarily determined by excess air ratio. The increased excess air ratio elevates in-cylinder oxygen content, promoting methanol combustion and reducing HC emissions as the excess air ratio ranges from 1.0 to 1.3. The HC concentration remains below 400 ppm under all spark timings when the excess air ratio is 1.3. At an excess air ratio of 1.35, combustion instability leads to elevated HC emissions. HC emissions are reduced by 74.8% at the spark timing of −33 °CA aTDC as the excess air ratio increases from 1.0 to 1.35.

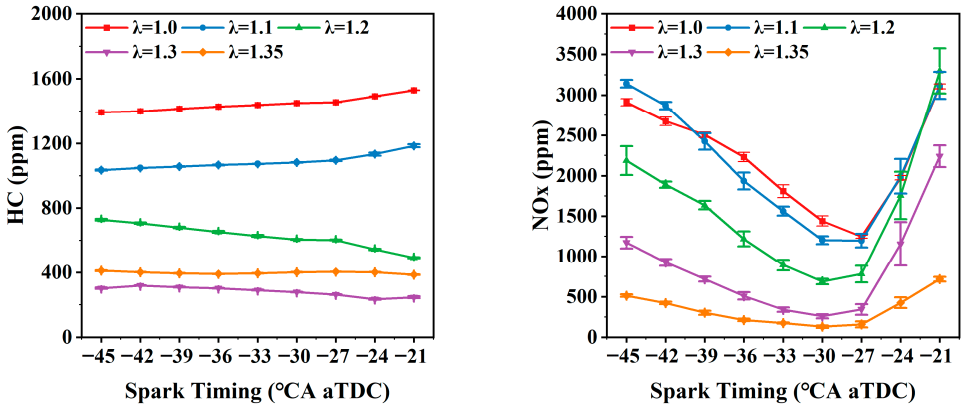


Figure 8. Effect of spark timing and excess air ratio on (**a**) HC and (**b**) NOx emissions.

Figure 8b presents the variation in NOx at different spark timings and excess air ratios. As spark timing advances, NOx emission initially decreases and then increases, typically reaching the minimum at spark timing of −27 °CA aTDC or −30 °CA aTDC. According to the Zeldovich mechanism, the formation rate of NOx is primarily determined by high temperature, pressure, and oxidation concentration. Although oxidation concentration is increased as the excess air ratio increases, the lean mixture significantly reduces the peak temperature in the cylinder [37], resulting in a 91.0% reduction in NOx emission at the spark timing of −30 °CA aTDC.

3.3. Machine Learning Modelling for Methanol Engine Performance

The original dataset contained 612 samples, of which 561 were retained for model training and validation after preprocessing and standardization. The predictive accuracy of four models for engine performance and emission characteristics is compared.

The comparison of predicted values based on SVM with experimental values for engine performance and emission characteristics is presented in Figure 9. The x-axis and y-axis represent the experimental and predicted values, respectively. For engine performance, the test data points are closely aligned with the line x = y, except for a few outliers. The slope of the fitted line approaches 1, and the R^2 values of brake torque, brake power, BTE, and BSFC all exceed 0.98, indicating high predictive accuracy of SVM. For emission characteristics, the slope of less than 1 for HC indicates an underestimation at higher HC emission levels. The R^2 values of HC and NOx both exceed 0.92, indicating that the predictive accuracy of SVM for emission characteristics remains satisfactory.

Figure 10 compares the predicted and actual values of the SVM model for engine performance and emission characteristics and presents the scatter plot comparing the experimental with predicted values based on SVM. The predicted values of performance features generally align with experimental values, with minor deviations observed at low values for brake torque and brake power and at high values for BSFC. The RMSE of brake torque, brake power, BTE, and BSFC are 1.0403 N·m, 0.1397 kW, 0.2389%, and 8.0469 g/kW·h, respectively. Prediction errors are relatively pronounced for HC emissions, with part of the HC data significantly deviating from predictions. The general trends for emissions remain largely consistent with experimental observations.

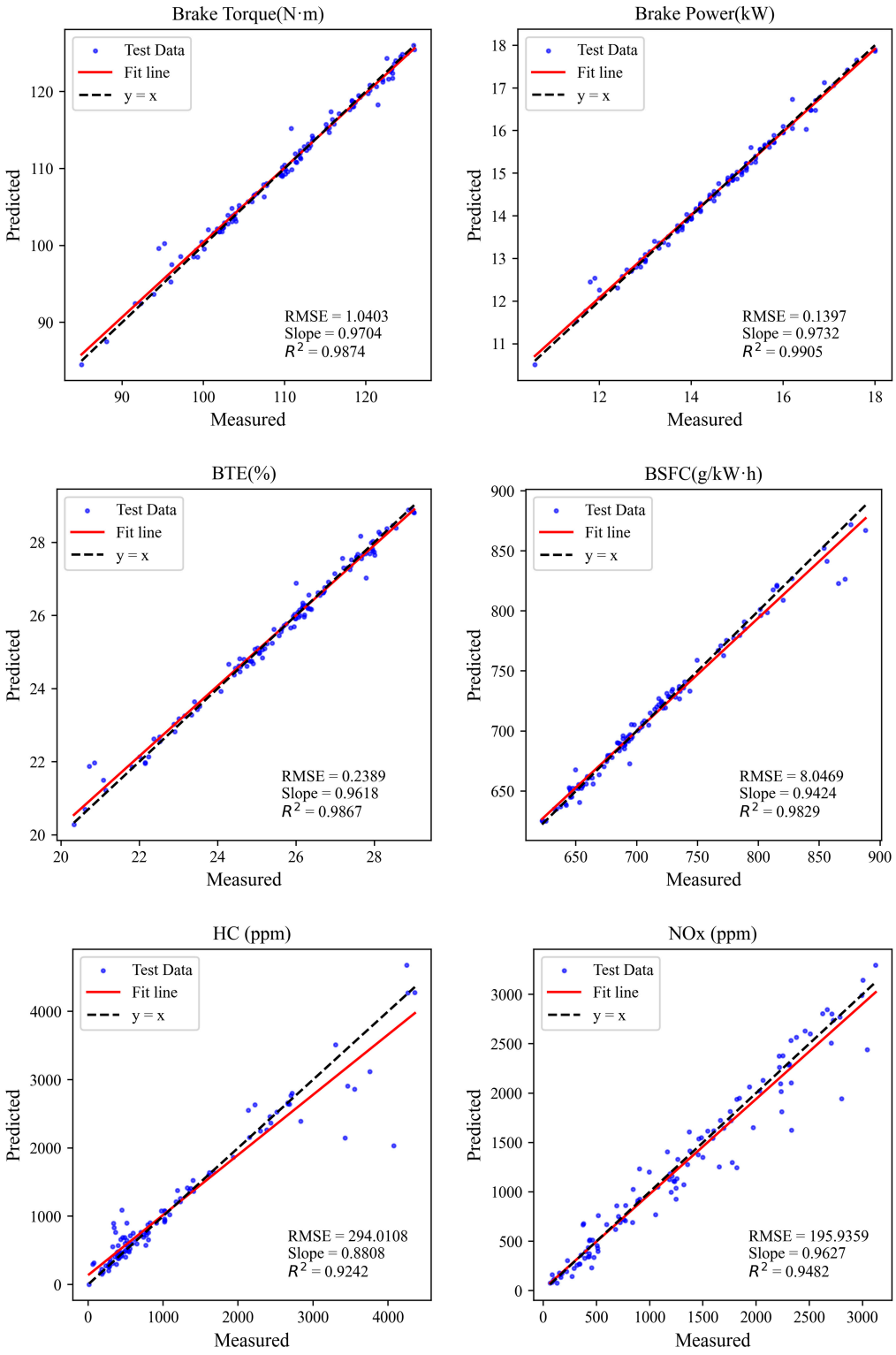


Figure 9. Linear regression plot between predicted and experimental values of SVM model for engine performance and emission characteristics.

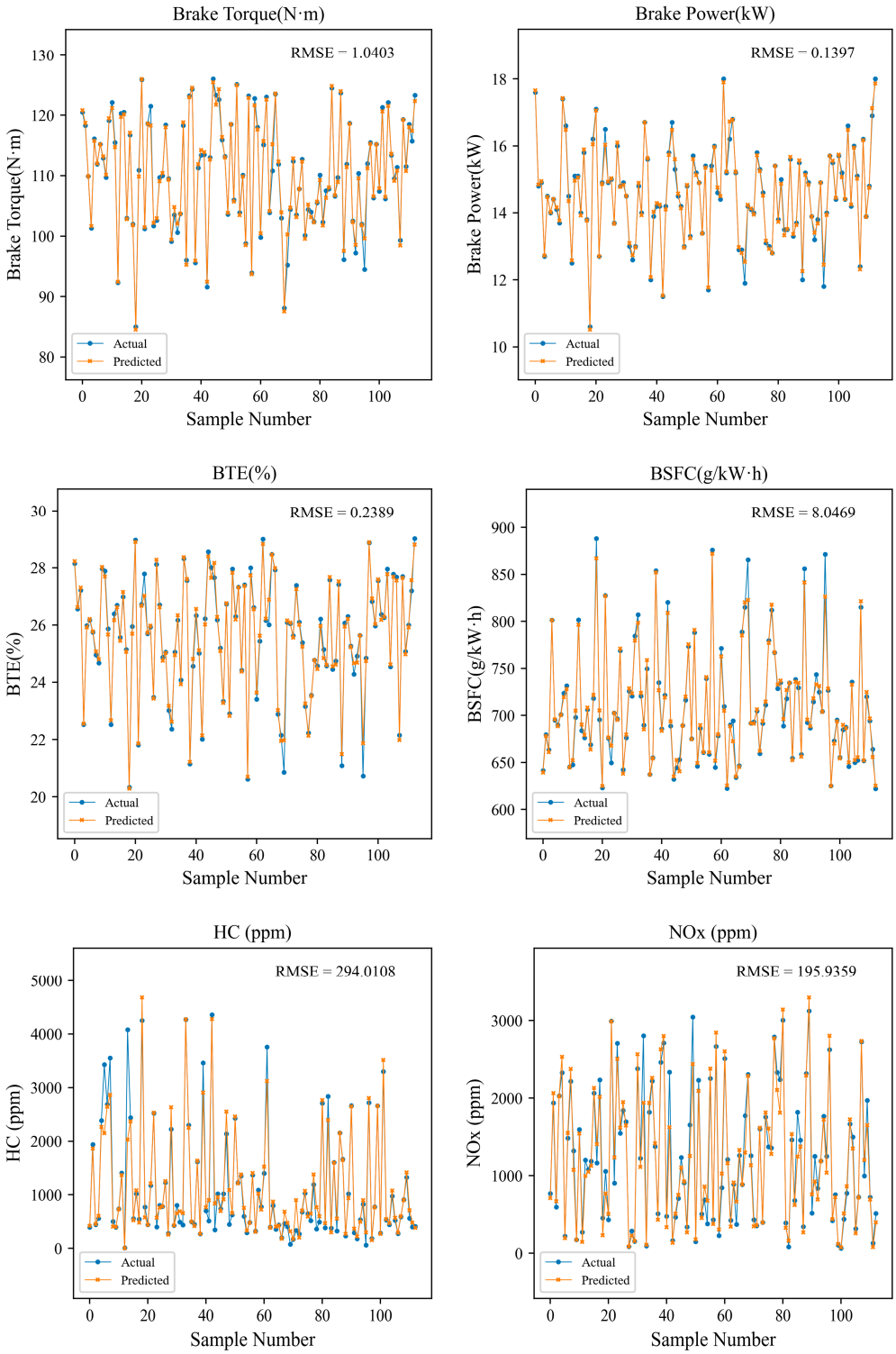


Figure 10. Comparison between predicted and actual values of SVM model for engine performance and emission characteristics.

Table 3 compares the R^2 and RMSE for each output parameter across four models. SVM demonstrates superior predictive accuracy for engine performance, attaining R^2 values exceeding 0.98 for brake torque, brake power, BTE, and BSFC, outperforming those of ANN, LightGBM, and RF. For emissions, the R^2 value for HC in the SVM is 0.9242, lower than those of LightGBM and RF but still within an acceptable range. The R^2 value for NOx in SVM is 0.9482, significantly higher than that of the other models. For ANN, LightGBM, and RF, the R^2 values for engine performance all exceed 0.92, exhibiting acceptable predictive accuracy.

LightGBM and RF exhibit high accuracy in predicting HC with the R^2 values of 0.9894 and 0.9486, respectively, while the R^2 value in ANN is 0.8541. The R^2 values for NOx emissions in ANN, LightGBM, and RF all exceed 0.83 but are lower than 0.9. Machine learning models, including SVM, ANN, LightGBM, and RF, all demonstrate reliable predictive accuracy for engine performance and emission characteristics. SVM exhibits the most favourable comprehensive performance, demonstrating superior ability to capture the nonlinear relationship between inputs and outputs with limited experimental datasets.

Table 3. Comparison of SVM, ANN, LightGBM, and RF models for output parameters.

	R^2				RMSE			
	SVM	**ANN**	**LightGBM**	**RF**	**SVM**	**ANN**	**LightGBM**	**RF**
Brake Torque (N·m)	0.9874	0.9496	0.9760	0.9245	1.0403	2.0818	1.4367	2.5469
Brake Power (kW)	0.9905	0.9802	0.9764	0.9516	0.1397	0.2016	0.2197	0.3147
BTE (%)	0.9867	0.9670	0.9806	0.9476	0.2389	0.3764	0.2886	0.4739
BSFC (g/kW·h)	0.9829	0.9573	0.9797	0.9379	8.0469	12.7104	8.7745	15.3364
HC (ppm)	0.9242	0.8541	0.9894	0.9486	294.0108	407.7730	110.1627	241.9497
NOx (ppm)	0.9482	0.8951	0.8687	0.8399	195.9359	278.8169	311.9660	344.5104

A 3-fold cross-validation was conducted to assess the robustness of the SVM model, and the MSE values are summarized in Table 4. Owing to the limited volume of experimental data, the MSE values are relatively high. The MSE values range from 0.02 to 0.08 for engine performance and from 0.2 to 0.4 for emissions. The MSE for each parameter shows minimal variation across folds, indicating that the SVM model demonstrates relatively high robustness on the current dataset.

Table 4. Results of 3-fold cross-validation for the SVM mode.

	Train MSE		
	Fold 1	**Fold 2**	**Fold 3**
Brake Torque (N·m)	0.0586	0.0524	0.0459
Brake Power (kW)	0.0355	0.0331	0.0272
BTE (%)	0.0639	0.0565	0.0465
BSFC (g/kW·h)	0.0765	0.0675	0.0614
HC (ppm)	0.3216	0.2687	0.2213
NOx (ppm)	0.2541	0.2147	0.2094

4. Conclusions

This study presents experimental and modelling investigations on the performance of an SI methanol marine engine operating under lean conditions. The effects of spark timing and excess air ratio on combustion characteristics, engine performance, and emissions are explored to improve the performance of the methanol marine engine. SVM, ANN, LightGBM, and RF are developed to predict engine performance and emissions characteristics. An accurate predictive machine model is provided to shorten experimental cycles. The main conclusions are as follows:

As spark timing advances, the combustion phase advances, with burn duration being extended. In addition, CA05 advances from after to before TDC, and the crank angle of CA90 remains nearly constant. When the excess air ratio is less than 1.35, IMEP and BTE reach their maximum at the optimal spark timing. The corresponding optimal spark timing exhibits an advancing tendency with increasing excess air ratio. The spark timing has little influence on the HC emission; however, a significant variation in HC emission is observed with increasing excess air ratio. NOx first decreases and then increases with the advance

in spark timing, typically reaching the minimum at spark timing of −27 °CA aTDC or −30 °CA aTDC.

SVM, ANN, LightGBM, and RF all exhibit high accuracy in predicting engine performance, with R^2 values for brake torque, brake power, BTE, and BSFC all exceeding 0.94. The trends of predicted data show strong agreement with experimental data. Compared with ANN, LightGBM, and RF, SVM achieves R^2 values exceeding 0.98 for engine performance and 0.92 for emission characteristics, indicating the most favourable comprehensive performance of SVM.

Future research will focus on further improving the thermal efficiency, extending the lean–burn limits, and achieving clean, efficient, and stable operation of methanol-fueled marine engines. More experimental data will be used to increase the accuracy of the predictive model.

Author Contributions: Conceptualization, S.G.; Methodology, S.G.; Investigation, S.G. and J.L.; Resources, S.G.; Data curation, S.G. and Z.F.; Writing—original draft, S.G. and W.L.; Writing—review & editing, S.G., W.L. and X.G.; Supervision, W.L. and X.G.; Funding acquisition, W.L. and X.G. All authors have read and agreed to the published version of the manuscript.

Funding: This research was funded by the "Pioneer and Leading Goose + X" R&D Program of Zhejiang (Grant No. 2025C01202(SD2)).

Data Availability Statement: The original contributions presented in this study are included in the article. Further inquiries can be directed to the corresponding author.

Conflicts of Interest: The authors declare no conflicts of interest.

References

1. Bortnowska, M. Projected reductions in CO_2 emissions by using alternative methanol fuel to power a service operation vessel. *Energies* **2023**, *16*, 7419. [CrossRef]
2. Kelleher, O.; Daly, C. Litigating the fit for 55 package: Statutory and rights-based challenges to national energy and climate plans as a means of implementing and/or enhancing the ambition of the EU's fit for 55 package. *Rev. Eur. Comp. Int. Environ. Law* **2025**, *34*, 49–61. [CrossRef]
3. Aakko-Saksa, P.T.; Lehtoranta, K.; Kuittinen, N.; Järvinen, A.; Jalkanen, J.-P.; Johnson, K.; Jung, H.; Ntziachristos, L.; Gagné, S.; Takahashi, C.; et al. Reduction in greenhouse gas and other emissions from ship engines: Current trends and future options. *Prog. Energy Combust. Sci.* **2023**, *94*, 101055. [CrossRef]
4. Gray, N.; McDonagh, S.; O'Shea, R.; Smyth, B.; Murphy, J.D. Decarbonising ships, planes and trucks: An analysis of suitable low-carbon fuels for the maritime, aviation and haulage sectors. *Adv. Appl. Energy* **2021**, *1*, 100008. [CrossRef]
5. Zhen, X.; Wang, Y.; Zhu, Y. Study of knock in a high compression ratio SI methanol engine using LES with detailed chemical kinetics. *Energy Convers. Manag.* **2013**, *75*, 523–531. [CrossRef]
6. Zhu, Z.; Mu, Z.; Wei, Y.; Du, R.; Guan, W.; Liu, S. Cylinder-to-cylinder variation of knock and effects of mixture formation on knock tendency for a heavy-duty spark ignition methanol engine. *Energy* **2022**, *254*, 124197. [CrossRef]
7. Zhang, M.; Hong, W.; Xie, F.; Liu, Y.; Su, Y.; Li, X.; Liu, H.; Fang, K.; Zhu, X. Effects of diluents on cycle-by-cycle variations in a spark ignition engine fueled with methanol. *Energy* **2019**, *182*, 1132–1140. [CrossRef]
8. Rao, X.; Yuan, C.; Guo, Z.; Xu, Y.; Sheng, C. Methanol as an alternative fuel for marine engines: A comprehensive review of current state, opportunities, and challenges. *Renew. Energy* **2025**, *252*, 123562. [CrossRef]
9. Zhu, Z.; Mu, Z.; Wei, Y.; Du, R.; Liu, S. Experimental evaluation of performance of heavy-duty SI pure methanol engine with EGR. *Fuel* **2022**, *325*, 124948. [CrossRef]
10. Chen, Z.; Wang, L.; Zeng, K. Comparative study of combustion process and cycle-by-cycle variations of spark-ignition engine fueled with pure methanol, ethanol, and n-butanol at various air–fuel ratios. *Fuel* **2019**, *254*, 115683. [CrossRef]
11. Kang, M.S.; Jeong, H.J.; Massoudi Farid, M.; Hwang, J. Effect of staged combustion on low NOx emission from an industrial-scale fuel oil combustor in south korea. *Fuel* **2017**, *210*, 282–289. [CrossRef]
12. Jung, D.; Iida, N. An investigation of multiple spark discharge using multi-coil ignition system for improving thermal efficiency of lean SI engine operation. *Appl. Energy* **2018**, *212*, 322–332. [CrossRef]

13. Zhao, H.; Qu, H.; Han, L.; Gong, Y.; Zhang, L.; Li, L.; Xie, F.; Qian, D. Effect of the miller cycle strategy on methanol and ethanol engines under stoichiometric combustion and lean burn. *Energy* **2025**, *327*, 136416. [CrossRef]
14. Kim, T.Y.; Park, C.; Oh, S.; Cho, G. The effects of stratified lean combustion and exhaust gas recirculation on combustion and emission characteristics of an LPG direct injection engine. *Energy* **2016**, *115*, 386–396. [CrossRef]
15. Gong, C.; Li, D.; Liu, J.; Liu, F. Numerical evaluation of ignition timing influences on performance of a stratified-charge H2/methanol dual-injection automobile engine under lean-burn condition. *Energy* **2024**, *290*, 130209. [CrossRef]
16. Duan, Q.; Kou, H.; Li, T.; Yin, X.; Zeng, K.; Wang, L. Effects of injection and spark timings on combustion, performance and emissions (regulated and unregulated) characteristics in a direct injection methanol engine. *Fuel Process. Technol.* **2023**, *247*, 107758. [CrossRef]
17. Ning, L.; Duan, Q.; Kou, H.; Zeng, K. Parametric study on effects of methanol injection timing and methanol substitution percentage on combustion and emissions of methanol/diesel dual-fuel direct injection engine at full load. *Fuel* **2020**, *279*, 118424. [CrossRef]
18. Yin, X.; Yue, G.; Liu, J.; Duan, H.; Duan, Q.; Kou, H.; Wang, Y.; Yang, B.; Zeng, K. Investigation into the operating range of a dual-direct injection engine fueled with methanol and diesel. *Energy* **2023**, *267*, 126625. [CrossRef]
19. Taheri-Garavand, A.; Heidari-Maleni, A.; Mesri-Gundoshmian, T.; Samuel, O.D. Application of artificial neural networks for the prediction of performance and exhaust emissions in IC engine using biodiesel-diesel blends containing quantum dot based on carbon doped. *Energy Convers. Manag. X* **2022**, *16*, 100304. [CrossRef]
20. Wang, H.; Ji, C.; Shi, C.; Ge, Y.; Wang, S.; Yang, J. Development of cyclic variation prediction model of the gasoline and n-butanol rotary engines with hydrogen enrichment. *Fuel* **2021**, *299*, 120891. [CrossRef]
21. Rahimi Molkdaragh, R.; Jafarmadar, S.; Khalilaria, S.; Soukht Saraee, H. Prediction of the performance and exhaust emissions of a compression ignition engine using a wavelet neural network with a stochastic gradient algorithm. *Energy* **2018**, *142*, 1128–1138. [CrossRef]
22. Wang, Y.; Xiao, G.; Li, B.; Tian, H.; Leng, X.; Wang, Y.; Dong, D.; Long, W. Study on the performance of diesel-methanol diffusion combustion with dual-direct injection system on a high-speed light-duty engine. *Fuel* **2022**, *317*, 123414. [CrossRef]
23. Ding, W.; Deng, J.; Wang, C.; Deng, R.; Yang, H.; Tang, Y.; Ma, Z.; Li, L. Operating and thermal efficiency boundary expansion of argon power cycle hydrogen engine. *Processes* **2023**, *11*, 1850. [CrossRef]
24. Nour, M.; Kosaka, H.; Bady, M.; Sato, S.; Abdel-Rahman, A.K. Combustion and emission characteristics of DI diesel engine fuelled by ethanol injected into the exhaust manifold. *Fuel Process. Technol.* **2017**, *164*, 33–50. [CrossRef]
25. Duan, X.; Li, Y.; Liu, Y.; Liu, J.; Wang, S.; Guo, G. Quantitative investigation the influences of the injection timing under single and double injection strategies on performance, combustion and emissions characteristics of a GDI SI engine fueled with gasoline/ethanol blend. *Fuel* **2020**, *260*, 116363. [CrossRef]
26. Beyfuss, B.; Flicker, L.; Gotthard, T.; Hofmann, P.; Zahradnik, F.; Krenn, C.; Lubich, G. *Evaluation of Spark-Ignited Kerosene Operation in a Wankel Rotary Engine*; SAE: Warrendale, PA, USA, 2021.
27. Shi, C.; Ji, C.; Wang, H.; Wang, S.; Yang, J.; Ge, Y. Comparative evaluation of intelligent regression algorithms for performance and emissions prediction of a hydrogen-enriched wankel engine. *Fuel* **2021**, *290*, 120005. [CrossRef]
28. Zhu, X.; Shen, X.; Chen, K.; Zhang, Z. Research on the prediction and influencing factors of heavy duty truck fuel consumption based on LightGBM. *Energy* **2024**, *296*, 131221. [CrossRef]
29. Cesar De Lima Nogueira, S.; Och, S.H.; Moura, L.M.; Domingues, E.; Coelho, L.D.S.; Mariani, V.C. Prediction of the NOx and CO_2 emissions from an experimental dual fuel engine using optimized random forest combined with feature engineering. *Energy* **2023**, *280*, 128066. [CrossRef]
30. Chen, Z.; He, J.; Chen, H.; Wang, L.; Geng, L. Experimental study of the effects of spark timing and water injection on combustion and emissions of a heavy-duty natural gas engine. *Fuel* **2020**, *276*, 118025. [CrossRef]
31. Yin, X.; Ma, B.; Wang, B.; Wu, F.; Hu, Q.; Duan, H.; Zeng, K. Optimizing air-fuel ratio for balancing thermal efficiency and emissions in a methanol direct injection engine under diverse operating conditions. *Energy* **2025**, *334*, 137547. [CrossRef]
32. Ji, C.; Wang, S.; Zhang, B. Effect of spark timing on the performance of a hybrid hydrogen–gasoline engine at lean conditions. *Int. J. Hydrogen Energy* **2010**, *35*, 2203–2212. [CrossRef]
33. Yin, X.; Xu, L.; Duan, H.; Wang, Y.; Wang, X.; Zeng, K.; Wang, Y. In-depth comparison of methanol port and direct injection strategies in a methanol/diesel dual fuel engine. *Fuel Process. Technol.* **2023**, *241*, 107607. [CrossRef]
34. Qian, L.; Wan, J.; Qian, Y.; Sun, Y.; Zhuang, Y. Experimental investigation of water injection and spark timing effects on combustion and emissions of a hybrid hydrogen-gasoline engine. *Fuel* **2022**, *322*, 124051. [CrossRef]
35. Ding, Y.; Pan, G.; Han, D.; Huang, Z. Combustion and emissions of an ammonia-gasoline dual-fuel spark ignition engine: Effects of ammonia substitution rate and spark ignition timing. *Int. J. Hydrogen Energy* **2025**, *122*, 348–358. [CrossRef]

36. İlhak, M.İ.; Tangöz, S.; Akansu, S.O.; Kahraman, N. An experimental investigation of the use of gasoline-acetylene mixtures at different excess air ratios in an SI engine. *Energy* **2019**, *175*, 434–444. [CrossRef]
37. Gong, C.; Yu, J.; Liu, F. Combined impact of excess air ratio and injection strategy on performances of a spark-ignition port- plus direct-injection dual-injection gasoline engine at half load. *Fuel* **2023**, *340*, 127605. [CrossRef]

Disclaimer/Publisher's Note: The statements, opinions and data contained in all publications are solely those of the individual author(s) and contributor(s) and not of MDPI and/or the editor(s). MDPI and/or the editor(s) disclaim responsibility for any injury to people or property resulting from any ideas, methods, instructions or products referred to in the content.